Amplitude analysis of $\gamma n \to \pi^- p$ data above 1 GeV

W. Chen,[1] H. Gao,[1] W. J. Briscoe,[2] D. Dutta,[3] A. E. Kudryavtsev,[2,4] M. Mirazita,[5] M. W. Paris,[2,6] P. Rossi,[5] S. Stepanyan,[7] I. I. Strakovsky,[2] V. E. Tarasov,[4] and R. L. Workman[2]

[1]*Duke University, Durham, North Carolina 27708, USA*
[2]*The George Washington University, Washington, DC 20052, USA*
[3]*Mississippi State University, Mississippi State, Mississippi 39762, USA*
[4]*Institute of Theoretical and Experimental Physics, Moscow, 117259 Russia*
[5]*INFN, Laboratori Nazionali di Frascati, 00044 Frascati, Italy*
[6]*Theory Division, Los Alamos National Laboratory, Los Alamos, New Mexico 87545, USA*
[7]*Thomas Jefferson National Accelerator Facility, Newport News, Virginia 23606, USA*

(Received 22 March 2012; revised manuscript received 26 May 2012; published 12 July 2012)

We report an extraction of nucleon resonance couplings using π^- photoproduction cross sections on the neutron. The world database for the process $\gamma n \to \pi^- p$ above 1 GeV has quadrupled with the addition of differential cross sections from the CEBAF Large Acceptance Spectrometer (CLAS) at Jefferson Lab in Hall B. Differential cross sections from CLAS have been improved with a final-state interaction determination using a diagrammatic technique taking into account the NN and πN final-state interaction amplitudes. Resonance couplings have been extracted and compared to previous determinations. With the addition of these cross sections significant changes are seen in the high-energy behavior of the Scattering Analysis Interactive Dial-in program cross sections and amplitudes.

DOI: 10.1103/PhysRevC.86.015206 PACS number(s): 13.60.Le, 24.85.+p, 25.10.+s, 25.20.−x

I. INTRODUCTION

High-precision data and new analysis techniques for $\gamma N \to \pi N$ are beginning to have a transformative impact on our understanding of the N and Δ resonance spectrum [1]. With the arrival of new and improved measurements of single- and double-polarization quantities, fits have become highly constrained. As a result, some multipole amplitudes and their underlying resonant components have changed significantly. This is particularly true for the neutron-target sector, where, until recently, there were few data on which to base fits and from which to extract $n\gamma$ photo-decay amplitudes.

The radiative decay width of the neutral N and Δ states may be extracted from π^- and π^0 photoproduction off a neutron, which involves a bound neutron target (typically the deuteron) and requires the use of a model-dependent nuclear correction. As a result, our knowledge of neutral resonance decays is less precise compared to the charged ones.

The existing database contains mainly $\gamma n \to \pi^- p$ differential cross sections [2]. Many of these are old bremsstrahlung measurements with limited angular coverages and large energy binnings. In several cases, the systematic uncertainties have not been given. At lower energies, there are data sets for the inverse π^- photoproduction reaction: $\pi^- p \to \gamma n$ [2]. This process is free from complications associated with a deuteron target. However, the disadvantage of using this reaction is the 5–500 times larger cross section for $\pi^- p \to \pi^0 n \to \gamma\gamma n$.

Here we explore the effect of adding CEBAF Large Acceptance Spectrometer (CLAS) differential cross sections for $\gamma n \to \pi^- p$, extracted from $\gamma d \to \pi^- pp$ [3], to the full Scattering Analysis Interactive Dial-in (SAID) program database. Measurements extend from 1.05 to 3.5 GeV in the photon energy. The present cross section set has quadrupled the world database for $\gamma n \to \pi^- p$ above 1 GeV, which allows for fits covering the region up to 2.7 GeV. We will show that these new data require large adjustments of our fits.

In Sec. II we will give a brief overview of the available experimental data. A discussion of the final-state interaction (FSI) calculations is given in Sec. III. The new CLAS data are compared with fits and older measurements in Sec. IV. In Sec. V, we discuss the fits and the extraction of resonance parameters. Finally, in Sec. VI, we summarize our findings and discuss the potential impact of future measurements and partial-wave analysis (PWA).

II. DATA SET

Due to lack of neutron targets, the database for the reactions $\gamma n \to \pi^0 n$ and $\gamma n \to \pi^- p$ is small compared to single-pion photoproduction reactions using proton targets, $\gamma p \to \pi^+ n$ and $\gamma p \to \pi^0 p$. Previous $\gamma N \to \pi N$ measurements are available in the SAID database [2]. A summary of experiments over the last 20 years is also provided [4–11].

Only 364 data-points are available for $\gamma n \to \pi^0 n$ below 2.7 GeV. For $\gamma n \to \pi^- p$, the situation is especially dire in the photon energy range above 1 GeV. There are only 360 data points, half of which come from polarized measurements. Below 1 GeV, there are significant numbers of $\gamma n \to \pi^- p$ data, coming mainly from Meson Factories (LAMPF, TRIUMF, and PSI) via inverse pion photoproduction $\pi^- p \to \gamma n$. Overall, there are 2093 data points, 17% of which are from polarized measurements. Some differential cross sections for the $\pi^- p \to \gamma n$ have been measured at BNL AGS, using the Crystal Ball multiphoton spectrometer. Measurements were made at 18 pion momenta from 238 to 748 MeV/c, corresponding to E_γ from 285 to 769 MeV [8]. These data

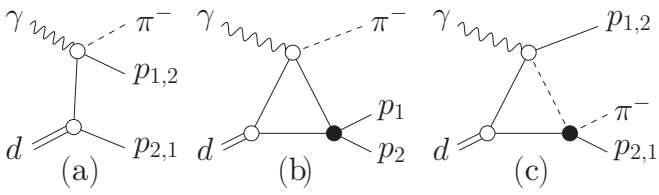

FIG. 1. Feynman diagrams for the leading components of the $\gamma d \to \pi^- pp$ amplitude. (a) IA, (b) pp-FSI, and (c) πN-FSI. Filled black circles show FSI vertices. Wavy, dashed, solid, and double lines correspond to the photons, pions, nucleons, and deuterons, respectively.

have been used to evaluate neutron multipoles in the vicinity of the $N(1440)1/2^+$ resonance.

We have recently considered the effect of the beam-asymmetry data (Σ) of $\vec{\gamma}n \to \pi^- p$ [11] and $\vec{\gamma}n \to \pi^0 n$ [12] from GRAAL on our fits to neutron-target data [13]. These include 216 Σ measurements of $\pi^0 n$ covering $E_\gamma = 703$–1475 MeV and $\theta = 53$–164° plus 99 Σ measurements of $\pi^- p$ for $E_\gamma = 753$–1439 MeV and $\theta = 33$–163°. Predictions for $\gamma n \to \pi^0 n$ were qualitatively different from the measurements over a wide angular range above a center-of-mass (CM) energy of 1650 MeV.

In 2009, the CLAS Collaboration at Jefferson Lab reported a detailed study of the reaction $\gamma n \to \pi^- p$ using a high statistics photoproduction experiment on deuterium [3]. This data set added 855 differential cross sections between 1.05 and 3.5 GeV, and pion production center-of-mass angles between 32° and 157°, to the existing data base. The overall systematic uncertainty varies between 5.8%, at the lowest photon energy, and up to 9.4% at the highest photon energy. Details of the data processing and analysis can be found in Ref. [14]. An improvement in the FSI has been made since the original publication [3].

Chen, *et al.* [3] estimated FSI corrections according to the Glauber formulation [15] and this correction was found to be about 20%. The uncertainty of the Glauber calculation for the FSI correction was estimated to be 5% in Refs. [9,10]. To study the model uncertainty in calculating the FSI correction, another calculation using the approach of Ref. [16] was adopted. Both methods agreed within 10%. A 10% systematic uncertainty to the differential cross section was assigned for the FSI correction [3].

In a further study of the FSI corrections for the $\gamma n \to \pi^- p$ cross section determination from the deuteron data, we used a diagrammatic technique [17], including the fact that CLAS does not detect protons with momenta less than 200 MeV/c. A short description of the FSI formalism is given in Sec. III.

III. FINAL-STATE INTERACTION CALCULATIONS

A. Amplitudes

Calculations of the $\gamma d \to \pi^- pp$ differential cross sections with the FSI taken into account, were done in a model represented by the diagrams in Fig. 1. These diagrams correspond to the IA [Fig. 1(a)], pp-FSI [Fig. 1(b)], and πN-FSI [Fig. 1(c)] amplitudes, denoted by M_a, M_b, and M_c, respectively. The resulting amplitude $M_{\gamma d}$ reads

$$M_{\gamma d} = M_a + M_b + M_c, \quad M_{a,c} = M_{a,c}^{(1)} + M_{a,c}^{(2)}. \tag{1}$$

IA and πN-FSI diagrams [Figs. 1(a), 1(c)] include also the cross terms between the final protons. The terms in Eq. (1) depend on the elementary $\gamma N \to \pi N$ amplitudes and deuteron wave function (DWF). The terms M_b and M_c depend also on the $NN \to NN$ and $\pi N \to \pi N$ amplitudes, respectively.

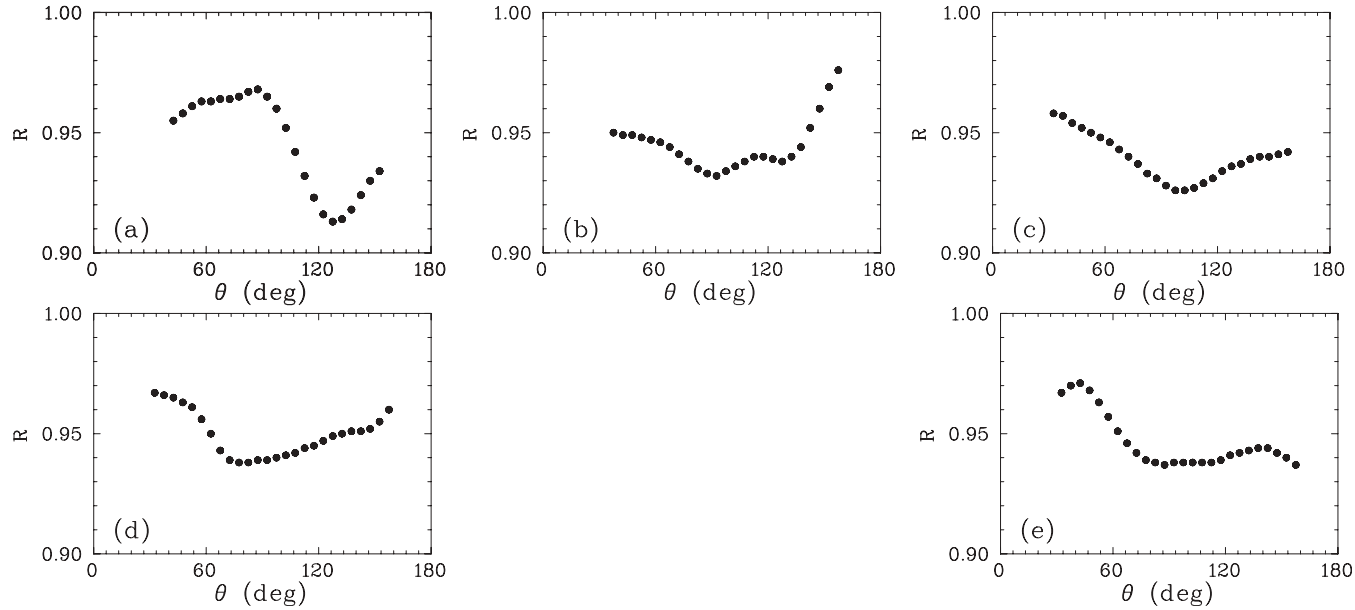

FIG. 2. FSI correction factor R for $\gamma n \to \pi^- p$ as a function of θ, where θ is the production angle of π^- in the CM frame. The present calculations (solid circles) are shown for five energies: (a) $E_\gamma = 1100$ MeV, (b) 1500 MeV, (c) 1900 MeV, (d) 2300 MeV, and (e) 2700 MeV. There are no uncertainties given.

The $\gamma N \to \pi N$ amplitudes were expressed through four independent Chew-Goldberger-Low-Nambu (CGLN) amplitudes [18] F_{1-4}, which were generated by the SAID code, using the George Washington University (GW) Data Analysis Center (DAC) pion photoproduction multipoles [19,20]. The NN- and πN-scattering amplitudes were calculated, using the results of GW NN [21] and πN [22] PWAs. The DWF was taken from the Bonn potential (full model) [23]. The elementary amplitudes are dependent on the momenta of the external and intermediate particles in Fig. 1. Thus, Fermi motion is taken into account in the $\gamma d \to \pi^- pp$ amplitude $M_{\gamma d}$. Details of calculations of the amplitudes $M_{a,b,c}$ in Eq. (1) are given in Ref. [17].

B. Final-state interaction correction

We extract the $\gamma n \to \pi^- p$ cross section from the deuteron data in the quasifree (QF) kinematical region of the $\gamma d \to \pi^- pp$ reaction with fast and slow protons p_1 and p_2, respectively, where the $\gamma d \to \pi^- pp$ cross section is dominated by the IA amplitude $M_a^{(1)}$ (i.e., $M_{\gamma d} \approx M_a^{(1)}$) while the cross term $M_a^{(2)}$ and the FSI amplitudes $M_{b,c}$ are relatively small. This consideration is addressed in the analysis of the CLAS [3,14] data for the reaction $\gamma d \to \pi^- pp$ with kinematical cuts $|\boldsymbol{p}_2| < 200\text{MeV}/c < |\boldsymbol{p}_1|$, corresponding to the CLAS experimental conditions. Hereafter, $\boldsymbol{p}_1$ ($\boldsymbol{p}_2$) stands for the laboratory three-momentum of fast (slow) proton p_1 (p_2).

In the QF approximation, the $\gamma d \to \pi^- pp$ and $\gamma n \to \pi^- p$ differential cross sections for unpolarized particles are related to each other in a known way [24].

$$\frac{d\sigma_{\gamma d}^{QF}}{d\,\boldsymbol{p}_2\,d\Omega} = \frac{E'_\gamma}{E_\gamma}\,\rho(|\boldsymbol{p}_2|)\,\frac{d\sigma_{\gamma n}}{d\Omega}. \tag{2}$$

Here Ω is the solid angle of relative motion in the $\pi^- p_1$ system, E_γ and $E'_\gamma = (1 + \beta\cos\theta_2)E_\gamma$ are the photon laboratory energies for the reactions $\gamma d \to \pi^- pp$ and $\gamma n \to \pi^- p$, respectively, $\beta = |\boldsymbol{p}_2|/E_2\,(\theta_2)$ is the laboratory velocity (polar angle) of spectator proton p_2, $\rho(|\boldsymbol{p}|)$ is the square of DWF, and $\int \rho(|\boldsymbol{p}|)\,d\,\boldsymbol{p} = 1$. Let $d\sigma_{\gamma d}^{QF}/d\Omega$ and $d\sigma_{\gamma d}/d\Omega$ be the deuteron cross section, integrated over $\boldsymbol{p}_2$ in a small region $|\boldsymbol{p}_2| < p_{\max}$ and obtained with the amplitudes $M_{\gamma d} = M_a^{(1)}$ and $M_a + M_b + M_c$, respectively. Then, from Eq. (2) (see details in Ref. [17]), we obtain

$$\frac{d\bar{\sigma}_{\gamma n}^{\text{exp}}}{d\Omega}(\bar{E}_\gamma, \theta) = c^{-1} R^{-1}(E_\gamma, \theta)\frac{d\sigma_{\gamma d}^{\text{exp}}}{d\Omega}(E_\gamma, \theta),$$
$$c = \int\limits_{|\boldsymbol{p}|<p_{\max}} \rho(|\boldsymbol{p}|)\,d\,\boldsymbol{p},\; R(E_\gamma, \theta) = \frac{d\sigma_{\gamma d}/d\Omega}{d\sigma_{\gamma d}^{QF}/d\Omega}, \tag{3}$$

were $d\bar{\sigma}_{\gamma n}^{\text{exp}}/d\Omega$ is the neutron cross section, extracted from the deuteron data. Here θ is the polar angle of the outgoing pion in the $\pi^- p_1$ frame, $c = c(p_{\max}) \leqslant 1$ is the effective number of neutrons with momenta $|\boldsymbol{p}| < p_{\max}$ in the deuteron, and R is the correction factor for FSI effects as well as for the suppressed amplitude $M_a^{(2)}$. The factor R depends on E_γ and θ as well as on the kinematical cuts applied.

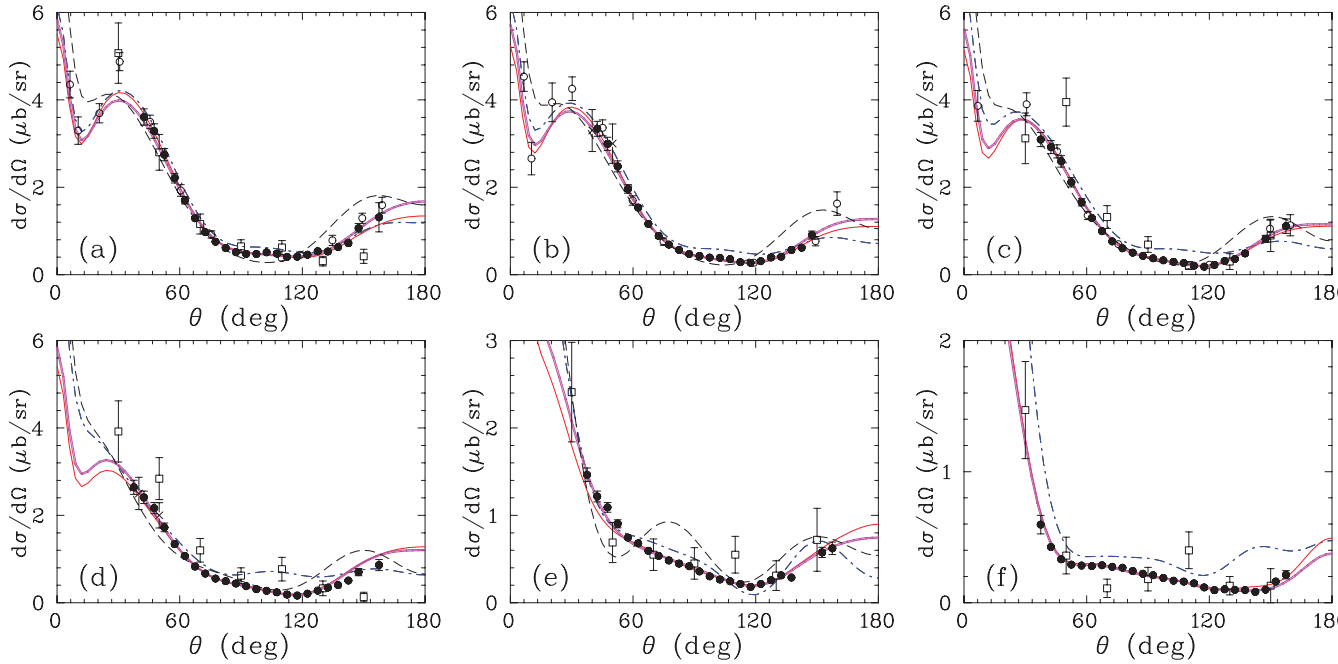

FIG. 3. (Color online) Differential cross sections for $\gamma n \to \pi^- p$ as a function of θ, where θ is the production angle of π^- in the CM frame. The present data (solid circles) are shown for six energy bins: (a) $E_\gamma = 1150$ MeV, (b) 1200 MeV, (c) 1250 MeV, (d) 1350 MeV, (e) 1550 MeV, and (f) 1900 MeV. Previous data are shown for experiments at SLAC [25] (open circles); DESY [26] (open squares), and Yerevan [27] (crosses). Plotted uncertainties are statistical only. Solid (dash-dotted) lines correspond to the GB12 (SN11 [13]) solution. Thick solid (dashed) lines give GZ12 solution (MAID07 [28], which terminates at $W = 2$ GeV).

The neutron cross section $d\bar{\sigma}_{\gamma n}/d\Omega$ (3) is averaged over the photon energy $E'_\gamma \sim E_\gamma$, and $\bar{E}_\gamma$ is some effective E'_γ value in the range $E_\gamma(1 \pm \beta)$. For small values of $p_{\max}$ we have $\beta \ll 1$ and $\bar{E}_\gamma \approx E_\gamma$.

We applied FSI corrections [17] dependent on the E_γ and θ. As an illustration, Fig. 2 shows the FSI correction factor R for the present $\gamma n \to \pi^- p$ differential cross sections as a function of the pion production angle in the CM frame for different energies over the range of the CLAS experiment. Overall, the FSI correction factor $R < 1$, while the effect [i.e., the $(1 - R)$ value] is less than 10% and the behavior is very smooth vs pion production angle.

The contribution of FSI calculations [17] to the overall systematics is estimated to be 2% (3%) below (above)

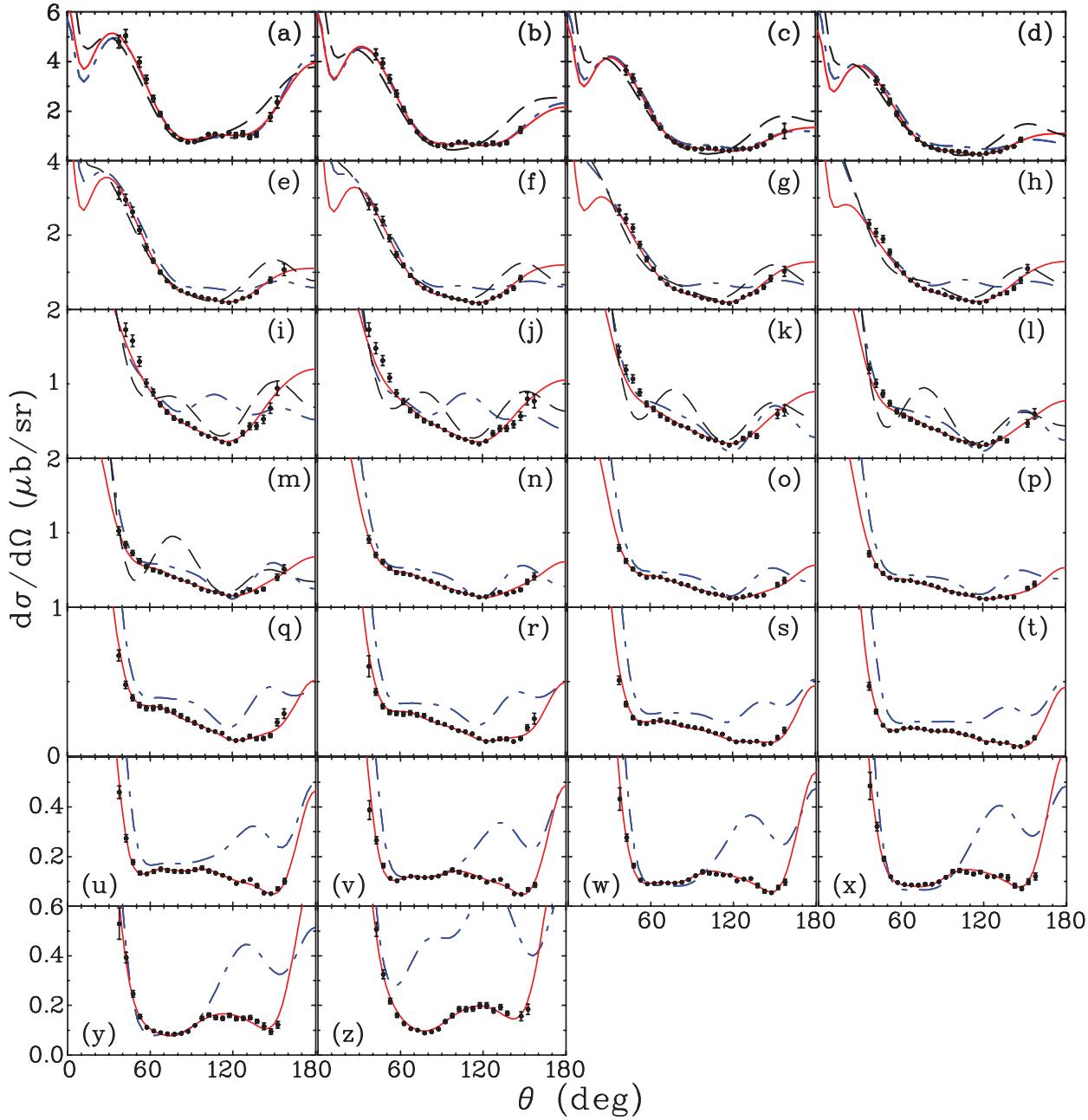

FIG. 4. (Color online) The differential cross section for $\gamma n \to \pi^- p$ below $E_\gamma = 2.7$ GeV versus pion CM angle. Solid (dash-dotted) lines correspond to the GB12 (SN11 [13]) solution. Dashed lines give the MAID07 [28] predictions. Experimental data are from the current (filled circles). Plotted uncertainties are statistical. (a) $E = 1050$ MeV, (b) $E = 1100$ MeV, (c) $E = 1150$ MeV, (d) $E = 1200$ MeV, (e) $E = 1250$ MeV, (f) $E = 1300$ MeV, (g) $E = 1350$ MeV, (h) $E = 1400$ MeV, (i) $E = 1450$ MeV, (j) $E = 1500$ MeV, (k) $E = 1550$ MeV, (l) $E = 1600$ MeV, (m) $E = 1650$ MeV, (n) $E = 1700$ MeV, (o) $E = 1750$ MeV, (p) $E = 1800$ MeV, (q) $E = 1850$ MeV, (r) $E = 1900$ MeV, (s) $E = 2000$ MeV, (t) $E = 2100$ MeV, (u) $E = 2200$ MeV, (v) $E = 2300$ MeV, (w) $E = 2400$ MeV, (x) $E = 2500$ MeV, (y) $E = 2600$ MeV, and (z) $E = 2700$ MeV.

1800 MeV. Above 2700 MeV, our estimation of systematic uncertainty due to the FSI calculations is 5%. Then we added FSI systematics to the overall experimental systematics in quadrature.

IV. RESULTS

Since the CLAS results for the $\gamma n \to \pi^- p$ differential cross sections consist of 855 experimental points, they are not tabulated in this or the previous [3] publication, but are available in the SAID database [2] along with their uncertainties and the energy binning.

Specific examples of agreement with previous measurements are displayed in Fig. 3, where we compare differential cross sections obtained here with those from SLAC [25], DESY [26], and Yerevan [27], at energies common to those experiments. Previous measurements used a modified Glauber approach and the procedure of unfolding the Fermi motion of the neutron target. The CLAS data and the results from SLAC, DESY, and Yerevan appear to agree well at these energies. Unfortunately, there are no measurements for $\pi^- p \to \gamma n$ to compare at these energies.

While agreement with previous measurements is generally good, the new data extend to higher energies with more complete angular coverage and are more constraining in the PWA, as is evident in Fig. 3.

A more complete comparison of the CLAS data with fits and predictions is given in Fig. 4. It is interesting to note that the data appear to have fewer angular structures than the earlier fits.

V. AMPLITUDE ANALYSIS OF DATA

We have included the new cross sections from the CLAS experiment in a number of multipole analyses covering incident photon energies up to 2.7 GeV, using the full SAID database, in order to gauge the influence of these measurements, as well as their compatibility with previous measurements.

In Table I, we compare the new GB12 and GZ12 solutions with four previous SAID fits (SN11 [13], SP09 [29], SM02 [19], and SM95 [30]). The overall χ^2 has remained stable against the growing database, which has increased by a factor of 2 since 1995 (most of this increase coming from data from photon-tagging facilities).

In fitting the data, the stated experimental systematic uncertainties have been used as an overall normalization adjustment factor for the angular distributions [13,19]. Presently, the pion photoproduction database below $E_\gamma = 2.7$ GeV consists of 26179 data points that have been fit in the GB12 (GZ12) solution with $\chi^2 = 54832$ (50998). The contribution to the total χ^2 in the GB12 (GZ12) analyses of the 626 new CLAS $\gamma n \to \pi^- p$ data points (e.g., those data points up to $E_\gamma = 2.7$GeV) is 1580 (1190). This should be compared to a starting $\chi^2 = 45636$ for the new CLAS data using predictions from our previous SN11 solution.

The solution, GB12, uses the same fitting form as our recent SN11 solution [13], which incorporated the neutron-target Σ data from GRAAL [11,12]. This fit form was motivated by a multichannel K-matrix approach, with an added phenomenological term proportional to the πN reaction cross section. A second fit, GZ12, used instead the recently proposed form [31] based on a unified Chew-Mandelstam parametrization of the GW DAC fits to both πN elastic scattering and photoproduction. This form explicitly includes contributions from channels πN, $\pi\Delta$, ρN, and ηN, as determined in the SAID elastic πN scattering analysis.

Using the relations quoted in Berends and Donnachie [32], we calculated resonance couplings, introduced in Copley *et al.* [33], from our electric and magnetic multipoles via the

TABLE I. χ^2 comparison of fits to pion photoproduction data up to 2.7 GeV. Results are shown for six different SAID solutions (current GB12 and GZ12 with previous SN11 [13], SP09 [29], SM02 [19], and SM95 [30]).

Solution	Energy limit (MeV)	χ^2/N_{Data}	N_{Data}
GZ12	2700	1.95	26179
GB12	2700	2.09	26179
SN11	2700	2.08	25553
SP09	2700	2.05	24912
SM02	2000	2.01	17571
SM95	2000	2.37	13415

TABLE II. Breit-Wigner resonance parameters [mass (W_R), full (Γ), and partial ($\Gamma_{\pi N}$) widths of resonances] associated with the SAID solution SP06 [22] obtained from πN scattering (second column) and neutron helicity amplitudes $A_{1/2}$ and $A_{3/2}$ (in [(GeV)$^{-1/2} \times 10^{-3}$] units) from the GB12 solution (first row), previous SN11 [13] solution (second row), and average values from the PDG10 [36] (third row). †See text.

Resonance	πN SAID	$A_{1/2}$	$A_{3/2}$
$N(1535)1/2^-$	$W_R = 1547$MeV	$-58 \pm 6^\dagger$	
	$\Gamma = 188$MeV	-60 ± 3	
	$\Gamma_{\pi N}/\Gamma = 0.36$	-46 ± 27	
$N(1650)1/2^-$	$W_R = 1635$MeV	$-40 \pm 10^\dagger$	
	$\Gamma = 115$MeV	-26 ± 8	
	$\Gamma_{\pi N}/\Gamma = 1.00$	-15 ± 21	
$N(1440)1/2^+$	$W_R = 1485$MeV	48 ± 4	
	$\Gamma = 284$MeV	45 ± 15	
	$\Gamma_{\pi N}/\Gamma = 0.79$	40 ± 10	
$N(1520)3/2^-$	$W_R = 1515$MeV	-46 ± 6	-115 ± 5
	$\Gamma = 104$MeV	-47 ± 2	-125 ± 2
	$\Gamma_{\pi N}/\Gamma = 0.63$	-59 ± 9	-139 ± 11
$N(1675)5/2^-$	$W_R = 1674$MeV	-58 ± 2	-80 ± 5
	$\Gamma = 147$MeV	-42 ± 2	-60 ± 2
	$\Gamma_{\pi N}/\Gamma = 0.39$	-43 ± 12	-58 ± 13
$N(1680)5/2^+$	$W_R = 1680$MeV	26 ± 4	-29 ± 2
	$\Gamma = 128$MeV	50 ± 4	-47 ± 2
	$\Gamma_{\pi N}/\Gamma = 0.70$	29 ± 10	-33 ± 9

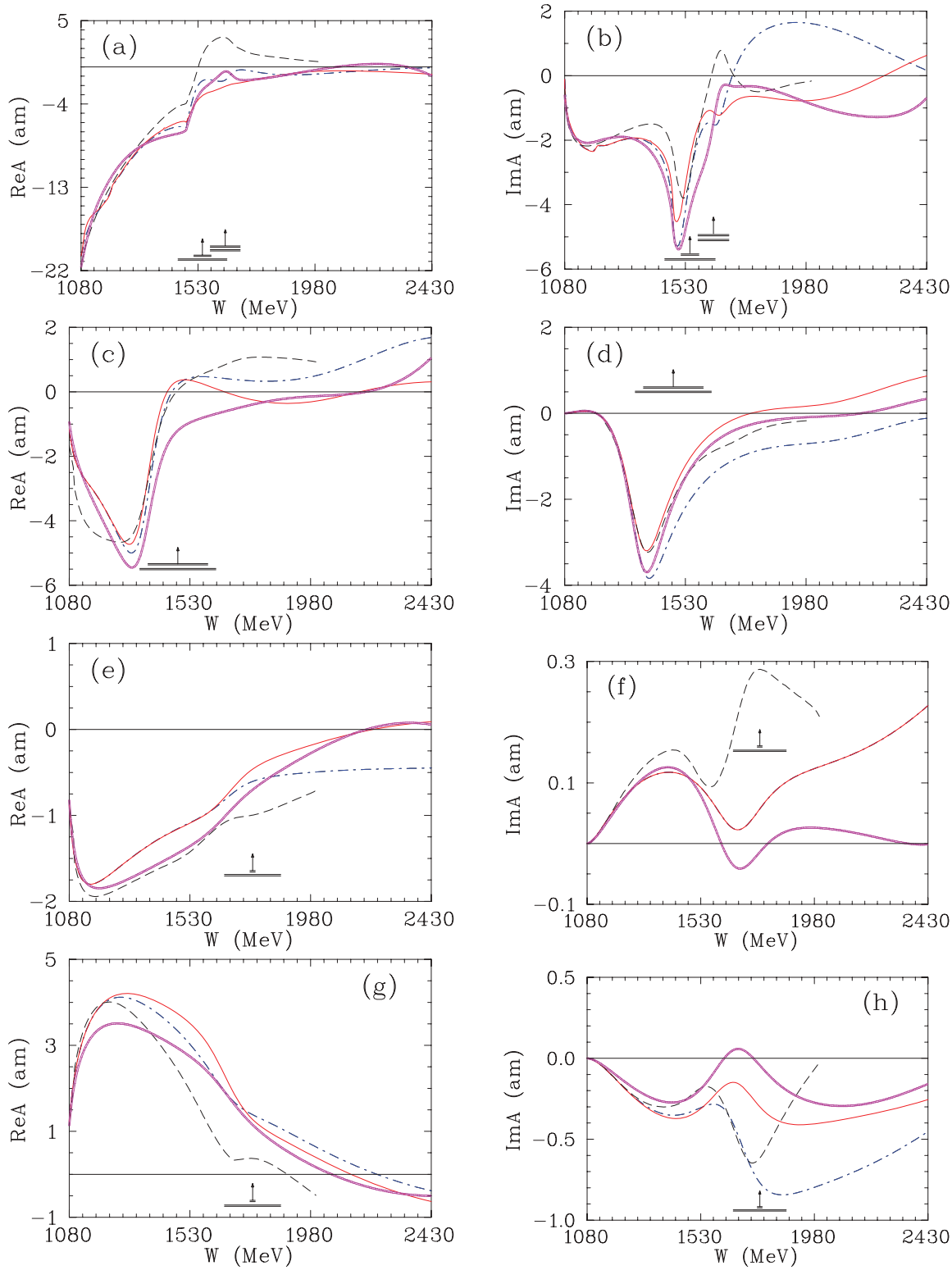

FIG. 5. (Color online) Neutron multipole $I = 1/2$ amplitudes from threshold to $W = 2.43$ GeV ($E_\gamma = 2.7$ GeV). Solid (dash-dotted) lines correspond to the GB12 (SN11 [13]) solution. Thick solid (dashed) lines give GZ12 solution (MAID07 [28], which terminates at $W = 2$ GeV). (a) Re$[_nE_{0+}^{1/2}]$, (b) Im$[_nE_{0+}^{1/2}]$, (c) Re$[_nM_{1-}^{1/2}]$, (d) Im$[_nM_{1-}^{1/2}]$, (e) Re$[_nE_{1+}^{1/2}]$, (f) Im$[_nE_{1+}^{1/2}]$, (g) Re$[_nM_{1+}^{1/2}]$, and (h) Im$[_nM_{1+}^{1/2}]$. Vertical arrows indicate mass (W_R), and horizontal bars show full (Γ) and partial ($\Gamma_{\pi N}$) widths of resonances extracted by the Breit-Wigner fit of the πN data associated with the SAID solution SP06 [22].

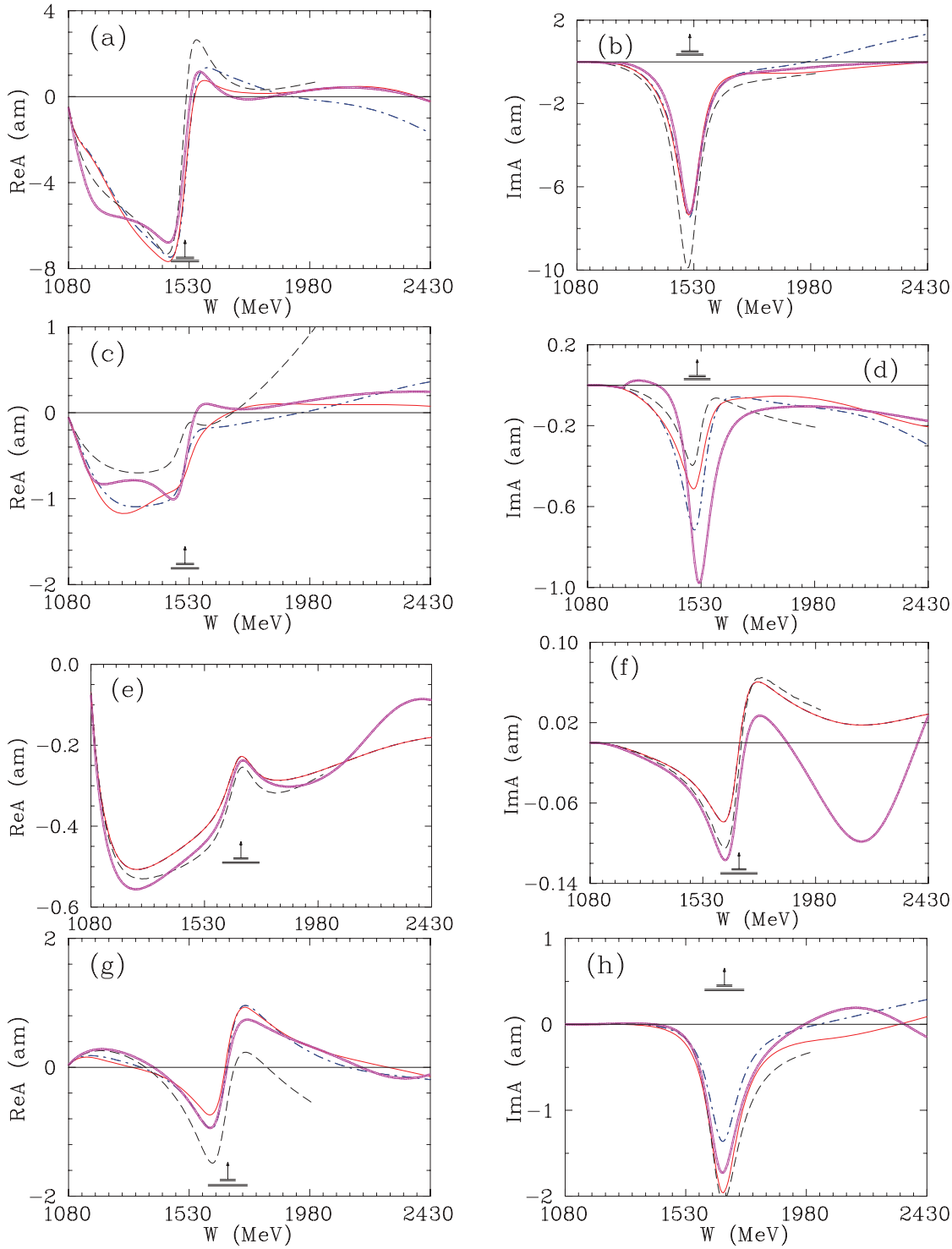

FIG. 6. (Color online) Notation of the multipoles is the same as in Fig. 5. (a) Re$[_n E^{1/2}_{2-}]$, (b) Im$[_n E^{1/2}_{2-}]$, (c) Re$[_n M^{1/2}_{2-}]$, (d) Im$[_n M^{1/2}_{2-}]$, (e) Re$[_n E^{1/2}_{2+}]$, (f) Im$[_n E^{1/2}_{2+}]$, (g) Re$[_n M^{1/2}_{2+}]$, and (h) Im$[_n M^{1/2}_{2+}]$.

relations [34],

$$A^{1/2}_{l+} = -\tfrac{1}{2}[(l+2)\bar{E}_{l+} + l\bar{M}_{l+}],$$
$$A^{3/2}_{l+} = -\tfrac{1}{2}\sqrt{l(l+2)}[\bar{E}_{l+} - \bar{M}_{l+}],$$
$$A^{1/2}_{(l+1)-} = -\tfrac{1}{2}[l\bar{E}_{(l+1)-} - (l+2)\bar{M}_{(l+1)-}],$$
$$A^{3/2}_{(l+1)-} = -\tfrac{1}{2}\sqrt{l(l+2)}[\bar{E}_{(l+1)-} + \bar{M}_{(l+1)-}],$$

where the above barred multipoles are related to our quoted amplitudes [35] (E,M) evaluated at Breit-Wigner resonance

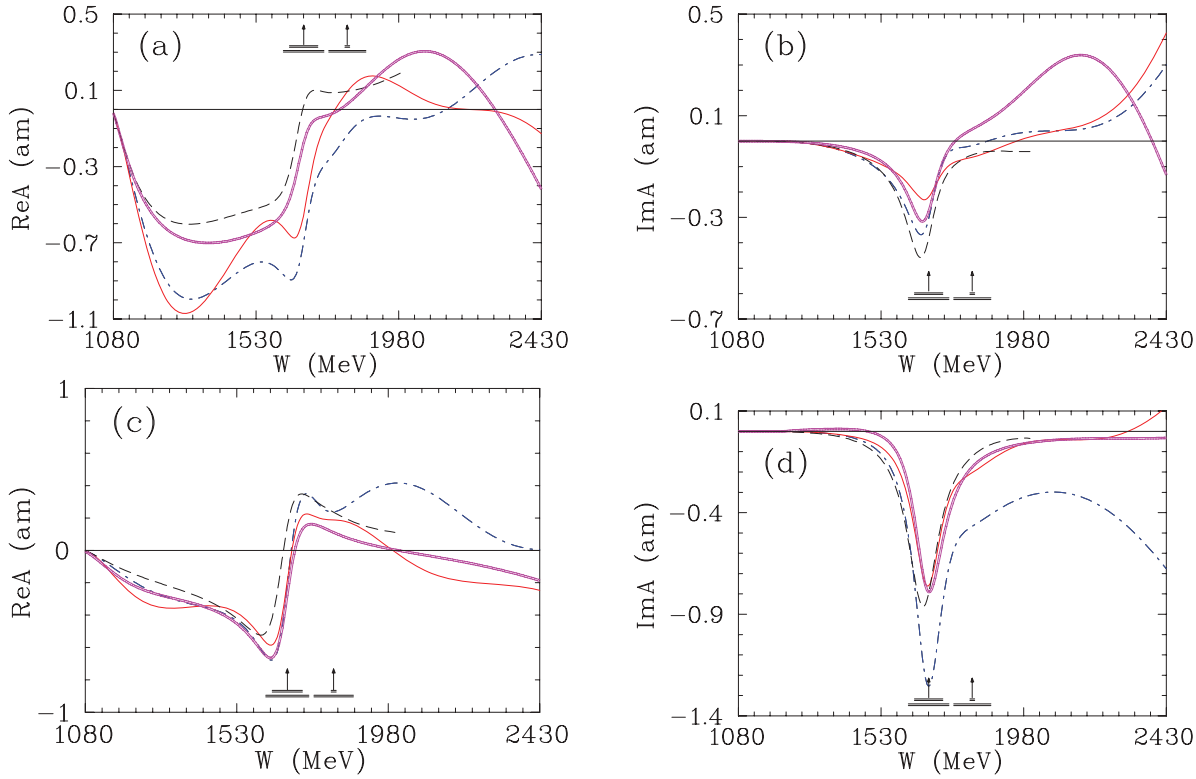

FIG. 7. (Color online) Notation of the multipoles is the same as in Fig. 5. (a) Re[$_nE_{3-}^{1/2}$], (b) Im[$_nE_{3-}^{1/2}$], (c) Re[$_nM_{3-}^{1/2}$], and (d) Im[$_nM_{3-}^{1/2}$].

energy (W_R) through the relation

$$(\bar{E}, \bar{M}) = C\left[\frac{(2j+1)\pi q_0 W_R \Gamma^2}{k_0 M_N \Gamma_{\pi N}}\right]^{1/2} \frac{(E, M)}{\hbar c}. \qquad (4)$$

The factor C in Eq. (4) is $\sqrt{\frac{2}{3}}$ for isospin $\frac{3}{2}$ and $-\sqrt{3}$ for isospin $\frac{1}{2}$ states. Here M_N is the nucleon mass, Γ and $\Gamma_{\pi N}$ are full and πN elastic widths, respectively. The variables q_0 and k_0 are, respectively, the center-of-mass pion and photon momenta at resonance energy (W_R). The resonance couplings defined in Ref. [32] and used in the manuscript are based on the Breit-Wigner (BW) parametrization of the amplitudes: the W_R, Γ, and $\Gamma_{\pi N}$ in Eq. (4) are the BW mass, full and πN partial widths of the resonance, respectively.

Resonance couplings extracted as in Ref. [13], are listed in Table II and compared to the previous SN11 determinations and the Particle Data Group (PDG) averages [36]. Couplings for the $N(1440)1/2^+$, $N(1520)3/2^-$, and $N(1675)5/2^-$ are reasonably close to the SN11 estimates. The value of $A_{1/2}$ found for the $N(1535)1/2^-$, using the GB12 fit, is very close to the SN11 determination. Using the GZ12 fit, however, the result is somewhat larger in magnitude (-85 ± 15). A similar feature was found for the proton couplings, using this form, in Ref. [31]. Using this alternate form, a determination of the $N(1650)1/2^- A_{1/2}$ was difficult and resulted in a value, lower in magnitude by about 50%, compared to the value from GB12 listed in Table II. For this reason, we consider the uncertainty associated with this state to be a lower limit only. No value was quoted for the $N(1720)3/2^+$ state. As can be seen in Figs. 5–7, the two different fit forms GB12 and GZ12, though similar in shape, have opposite signs for the imaginary parts of corresponding multipoles ($_nE_{1+}^{1/2}$ and $_nM_{1+}^{1/2}$) in the neighborhood of the resonance position, and even the sign can not be determined. This is in line with the PDG estimates, which also fail to give signs for the couplings to this state.

VI. SUMMARY AND CONCLUSION

A comprehensive set of differential cross sections at 26 energies for negative-pion photoproduction on the neutron, via the reaction $\gamma d \to \pi^- pp$, have been determined with a JLab tagged-photon beam for incident photon energies from 1.05 to 3.5 GeV. To accomplish a state-of-the-art analysis, we included FSI corrections using a diagrammatic technique, taking into account a kinematical cut with momenta less (more) than 200 MeV/c for slow (fast) outgoing protons.

The updated PWAs examined mainly the effect of new CLAS neutron-target data on the SAID multipoles and resonance parameters. These new data have been included in a SAID multipole analysis, resulting in new SAID solutions, GB12 and GZ12. A major accomplishment of this CLAS experiment is a substantial improvement in the π^--photoproduction database, adding 855 new differential cross sections quadrupling the world database for $\gamma n \to \pi^- p$ above 1 GeV. Comparison to earlier SAID fits, and a lower-energy fit

from the Mainz group, shows that the new solutions are much more satisfactory at higher energies.

On the experimental side, further improvements in the PWAs await more data, specifically in the region above 1 GeV, where the number of measurements for this reaction is small. Of particular importance in all energy regions is the need for data obtained involving polarized photons and polarized targets. Due to the closing of hadron facilities, new $\pi^- p \to \gamma n$ experiments are not planned and only $\gamma n \to \pi^- p$ measurements are possible at electromagnetic facilities using deuterium targets. Our agreement with existing π^- photoproduction measurements leads us to believe that these photoproduction measurements are reliable despite the necessity of using a deuterium target. We hope that new CLAS Σ-beam asymmetry measurements for $\vec{\gamma} n \to \pi^- p$, at $E_\gamma = 910$ up to 2400 MeV and pion production angles from 20° to 140° (1200 data) in the CM frame, will soon [37] provide further constraints for the neutron multipoles.

ACKNOWLEDGMENTS

The authors acknowledge helpful comments and preliminary fits from R. A. Arndt in the early stages of this work. Then the authors are thankful to E. Pasyuk for useful discussions. We acknowledge the outstanding efforts of the CLAS Collaboration who made the experiment possible. This work was supported in part by the US Department of Energy, Grants No. DE-FG02-99ER41110 and No. DE-FG02-03ER41231, by the Russian RFBR Grant No. 02-0216465, by the Russian Atomic Energy Corporation "Rosatom" Grant No. NSb-4172.2010.2, the National Science Foundation, and the Italian Istituto Nazionale di Fisica Nucleare.

[1] B. Krusche and S. Schadmand, Prog. Part. Nucl. Phys. **51**, 399 (2003); E. Klempt and J.-M. Richard, Rev. Mod. Phys. **82**, 1095 (2010); I. G. Aznauryan and V. D. Burkert, Prog. Part. Nucl. Phys. **67**, 1 (2012).
[2] W. J. Briscoe, I. I. Strakovsky, and R. L. Workman, Institute of Nuclear Studies of The George Washington University Database; [http://gwdac.phys.gwu.edu/analysis/pr_analysis.html] (unpublished).
[3] W. Chen *et al.* (CLAS Collaboration), Phys. Rev. Lett. **103**, 012301 (2009).
[4] M. Wang, Ph.D. thesis, University of Kentucky, 1992 (unpublished).
[5] K. Liu, Ph.D. thesis, University of Kentucky, 1994 (unpublished).
[6] J. C. Stasko *et al.*, Phys. Rev. Lett. **72**, 973 (1994).
[7] A. M. Sandorfi (private communication).
[8] A. Shafi, S. Prakhov, I. I. Strakovsky, W. J. Briscoe, B. M. K. Nefkens *et al.* (Crystal Ball Collaboration), Phys. Rev. C **70**, 035204 (2004).
[9] L. Y. Zhu *et al.* (Jefferson Lab Hall A Collaboration), Phys. Rev. Lett. **91**, 022003 (2003).
[10] L. Y. Zhu *et al.* (Jefferson Lab Hall A Collaboration), Phys. Rev. C **71**, 044603 (2005).
[11] G. Mandaglio *et al.* (GRAAL Collaboration), Phys. Rev. C **82**, 045209 (2010).
[12] R. Di Salvo *et al.* (GRAAL Collaboration), Eur. Phys. J. A **42**, 151 (2009).
[13] R. L. Workman, W. J. Briscoe, M. W. Paris, and I. I. Strakovsky, Phys. Rev. C **85**, 025201 (2012).
[14] W. Chen, Ph.D. thesis, Duke University, 2010 (unpublished).
[15] H. Gao, R. J. Holt, and V. R. Pandharipande, Phys. Rev. C **54**, 2779 (1996).
[16] J. M. Laget, Phys. Rev. C **73**, 044003 (2006).
[17] V. E. Tarasov, W. J. Briscoe, H. Gao, A. E. Kudryavtsev, and I. I. Strakovsky, Phys. Rev. C **84**, 035203 (2011).
[18] G. F. Chew, M. L. Goldberger, F. E. Low, and Y. Nambu, Phys. Rev. **106**, 1345 (1957).
[19] R. A. Arndt, W. J. Briscoe, I. I. Strakovsky, and R. L. Workman, Phys. Rev. C **66**, 055213 (2002).
[20] M. Dugger, J. P. Ball, P. Collins, E. Pasyuk, B. G. Ritchie, R. A. Arndt, W. J. Briscoe, I. I. Strakovsky, R. L. Workman *et al.* (CLAS Collaboration), Phys. Rev. C **76**, 025211 (2007).
[21] R. A. Arndt, W. J. Briscoe, I. I. Strakovsky, and R. L. Workman, Phys. Rev. C **76**, 025209 (2007).
[22] R. A. Arndt, W. J. Briscoe, I. I. Strakovsky, and R. L. Workman, Phys. Rev. C **74**, 045205 (2006).
[23] R. Machleidt, K. Holinde, and C. Elster, Phys. Rep. **149**, 1 (1987).
[24] I. Blomqvist and J. M. Laget, Nucl. Phys. A **280**, 405 (1977).
[25] P. E. Scheffler *et al.*, Nucl. Phys. B **75**, 125 (1974).
[26] P. Benz *et al.*, Nucl. Phys. B **65**, 158 (1973).
[27] L. O. Abrahamian *et al.*, Sov. J. Nucl. Phys. **32**, 69 (1980).
[28] D. Drechsel, S. S. Kamalov, and L. Tiator, Eur. Phys. J. A **34**, 69 (2007); [http://www.kph.uni-mainz.de/MAID/].
[29] M. Dugger, J. P. Ball, P. Collins, E. Pasyuk, B. G. Ritchie, R. A. Arndt, W. J. Briscoe, I. I. Strakovsky, R. L. Workman *et al.* (CLAS Collaboration), Phys. Rev. C **79**, 065206 (2009).
[30] R. A. Arndt, I. I. Strakovsky, and R. L. Workman, Phys. Rev. C **53**, 430 (1996).
[31] R. L. Workman, M. W. Paris, W. J. Briscoe, and I. I. Strakovsky, [Phys. Rev. C **85** (to be published 2012)].
[32] F. A. Berends and A. Donnachie, Nucl. Phys. B **136**, 317 (1978).
[33] L. A. Copley, G. Karl, and E. Obryk, Nucl. Phys. B **13**, 303 (1969).
[34] R. A. Arndt, R. L. Workman, Zhujun Li, and L. D. Roper, Phys. Rev. C **42**, 1864 (1990).
[35] R. A. Arndt, R. L. Workman, Zhujun Li, and L. D. Roper, Phys. Rev. C **42**, 1853 (1990).
[36] K. Nakamura *et al.* (Particle Data Group), J. Phys. G **37**, 075021 (2010).
[37] D. Sokhan, Ph.D. thesis, Edinburgh University, 2009 (unpublished).